Seismically detected cratering on Mars: Enhanced recent impact flux?

Ingrid Daubar, Raphaël Garcia, Alexander Stott, Benjamin Fernando, Gareth Collins, Colin Dundas, Natalia Wójcicka, Géraldine Zenhäusern, Alfred Mcewen, Simon Stähler, et al.

PLANETARY SCIENCE

Seismically detected cratering on Mars: Enhanced recent impact flux?

Ingrid J. Daubar[1]*, Raphaël F. Garcia[2], Alexander E. Stott[2], Benjamin Fernando[3], Gareth S. Collins[4], Colin M. Dundas[5], Natalia Wójcicka[4], Géraldine Zenhäusern[6], Alfred S. McEwen[7], Simon C. Stähler[6], Matthew Golombek[8], Constantinos Charalambous[4], Domenico Giardini[6], Philippe Lognonné[9], W. Bruce Banerdt[8]

Seismic observations of impacts on Mars indicate a higher impact flux than previously measured. Using six confirmed seismic impact detections near the NASA InSight lander and two distant large impacts, we calculate appropriate scalings to compare these rates with lunar-based chronology models. We also update the impact rate from orbital observations using the most recent catalog of new craters on Mars. The snapshot of the current impact rate at Mars recorded seismically is higher than that found using orbital detections alone. The measured rates differ between a factor of 2 and 10, depending on the diameter, although the sample size of seismically detected impacts is small. The close timing of the two largest new impacts found on Mars in the past few decades indicates either a heightened impact rate or a low-probability temporal coincidence, perhaps representing recent fragmentation of a parent body. We conclude that seismic methods of detecting current impacts offer a more complete dataset than orbital imaging.

INTRODUCTION

Impact cratering is an ongoing process continuously modifying planetary surfaces throughout the Solar System. Knowledge of the recent impact rate, even if only over a narrow window in time, can be applied to chronology systems to help calibrate crater count–based estimates of surface ages [e.g., (*1*, *2*)]. These are a valuable addition to other methods such as radioisotope dating of returned samples, which are limited by available materials. The nature of the current impact flux is also important in terms of understanding the physical processes modifying planetary surfaces now and in the past and for understanding the cosmic environment of the inner Solar System as an exploration and terrestrial hazard [e.g., (*3*, *4*)]. Examples of the implications of this work for that area are the orbital evolution of impactor reservoirs and breakup events of parent bodies.

New craters on Mars are detected by comparing repeat images of the surface to identify albedo changes indicative of newly formed impact sites (*5*–*7*). These have recently been cataloged, including crater diameters and before and after images constraining their formation time (*7*). Those data can now be used to calculate an updated impact rate using methods of Daubar *et al.* (*6*) applied to a broader range of time and diameter and with updated debiasing techniques.

Recently, new impacts have also been found on Mars using seismic data from the Seismic Experiment for Interior Structure (SEIS) (*8*) on the NASA InSight lander (*9*). Using a combination of seismic indicators that allowed estimation of the distances and azimuths of the events (*10*, *11*), plus orbital imaging searches, positive identifications were made of new craters at the predicted locations and constrained with images to have formed within a window of time containing the seismic signals (Fig. 1). Thus, the formation of these craters was established to be responsible for the seismic events. Short-range detections using dispersive acoustic signals located four impact sites near InSight (*10*, *11*). All of these are less than 289 km from the lander. Two very distant (teleseismic) detections of large marsquakes by the InSight Mars Quake Service (*12*) led to the discovery of two unusually large impact events (130 to 150 m in diameter craters) (*13*). Whether or not these large events were actually statistically unusual is one of the questions we address in this work. Premission estimates of impact detection rate were lower than the rate implied by these eight impact detections, although at least one order of magnitude uncertainty was associated with those initial estimates (*14*). Observational biases of seismic detections differ from those of orbital image–based searches; we discuss those biases and how we account for them to directly compare resulting equivalent current impact rates from these different datasets.

RESULTS

We present two datasets of confirmed new Martian craters: one identified seismically by the InSight mission and confirmed by orbital imaging and another based solely on orbital detection of date-constrained impact sites by the Context camera (CTX) on the Mars Reconnaissance Orbiter (MRO). Each dataset was scaled separately to an area-time factor (ATF) that represents the total possible time and area over which a search could have been considered to be complete (see Materials and Methods). The resulting equivalent annual impact rates are shown in Fig. 2 and compared to previously published isochrons.

For craters with diameters > ~10 m, impact rates using updated orbitally constrained impact crater (CTX-CTX–2023) (*7*) are higher but within error bars of those measured using a smaller dataset previously reported (CTX-CTX–2014) (*15*). At smaller diameters,

[1]Department of Earth, Environmental, and Planetary Sciences, Brown University, Providence, RI 02912, USA. [2]Institut Supérieur de l'Aéronautique et de l'Espace (ISAE-SUPAERO), Université de Toulouse, 10 Avenue Edouard Belin, 31400 Toulouse, France. [3]Department of Physics, University of Oxford, Oxford OX1 2JD, UK. [4]Imperial College London, South Kensington Campus, London SW7 2AZ, UK. [5]U.S. Geological Survey, Astrogeology Science Center, 2255 N. Gemini Dr, Flagstaff, AZ 86001, USA. [6]Institute of Geophysics, ETH Zürich, Sonneggstrasse 5, 8092 Zürich, Switzerland. [7]Lunar and Planetary Laboratory, University of Arizona, Tucson, AZ 85721, USA. [8]Jet Propulsion Laboratory, California Institute of Technology, Pasadena, CA 91109, USA. [9]Université Paris Cité, Institut de Physique du Globe de Paris, CNRS, F-75005 Paris, France.
*Corresponding author. Email: ingrid_daubar@brown.edu

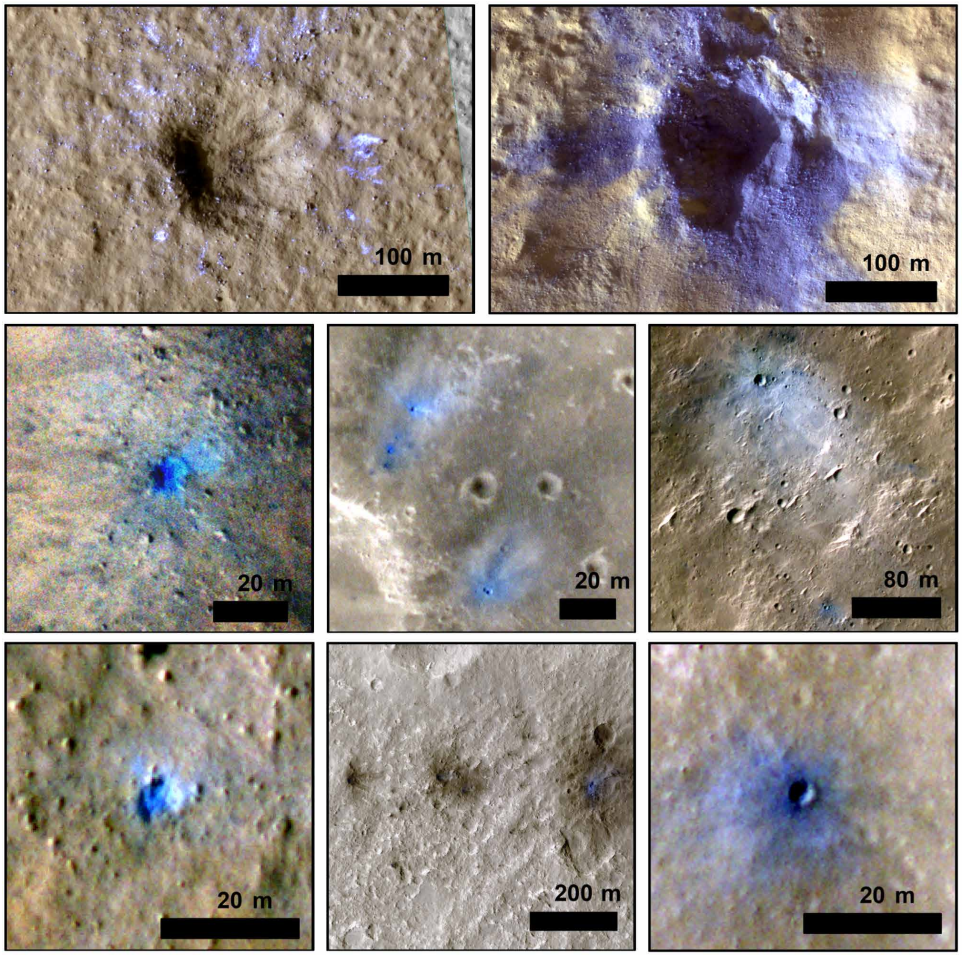

Fig. 1. HiRISE images of new impact craters detected in InSight seismic data. Excerpts from enhanced color RDR products. Full RED images inset for two large impacts (**top row**). Note that scale bars differ between images. North is up, and images have been stretched for contrast. Images: NASA/JPL/University of Arizona. For details, see Table 1.

impact rates measured with the updated data are slightly lower than those measured from the first part of the MRO mission (Fig. 2).

Seismically detected impacts show evidence of a significantly higher cratering rate at Mars than was previously documented using orbital images alone, although the sample size of seismically detected impacts is small. The measured rates differ between a factor of 2 and 10, depending on the diameter (Fig. 2). The density of small (D ~ 1 to 10 m) impacts near InSight and that of larger (D ~ 100 to 200 m), more distant impacts are both remarkably close to the commonly used martian cratering rate models of Hartmann and Daubar (*2*). The annualized impact rate for the seismically detected impacts is not far from the 1-year isochron for Mars based on radiometrically calibrated lunar cratering densities (*2*, *16*), especially when the uncertainty in those absolute ages is considered [estimated as a factor of 2 to 8 (*2*)]. The InSight-detected cratering rate is also consistent with recent models of small crater formation on Mars that account for atmospheric entry effects and assume a meteoroid flux based on terrestrial fireball observations and a Mars/Earth impactor flux ratio of 1.3 to 1.6 (*17*, *18*) . The nearby impacts follow nearly the same slope as model predictions, which have been adjusted for atmospheric loss (*16*).

The flattening of the cumulative curve (rollover of the differential curve) at small diameters (D < 10 m) in the orbital detections is not present in the seismic detections (Fig. 2, left). For the two large, distant impacts, the resulting rate is either much higher than or very close to the model predictions, depending on whether the two distant impacts are scaled to the timeframe of the InSight mission (3.1 Earth years) or MRO observations (16.1 Earth years).

DISCUSSION

Considering first only the orbitally detected impacts (brown symbols in Fig. 2), these results indicate that the impact rate over the timespan of the MRO data used (2006 to 2021) is lower than that measured previously using only the first part of the mission's data (2006 to 2013). If this difference reflects the real impact rate, then it could point to short-term variability. However, it is more likely that the orbital dataset has been incompletely searched using manual methods. The InSight-MRO collaboration demonstrated that, even when an impact location is fairly well constrained from seismic data, it can be difficult to identify the impact site in orbital images [e.g., the impact for seismic event S1034a was partially obscured by

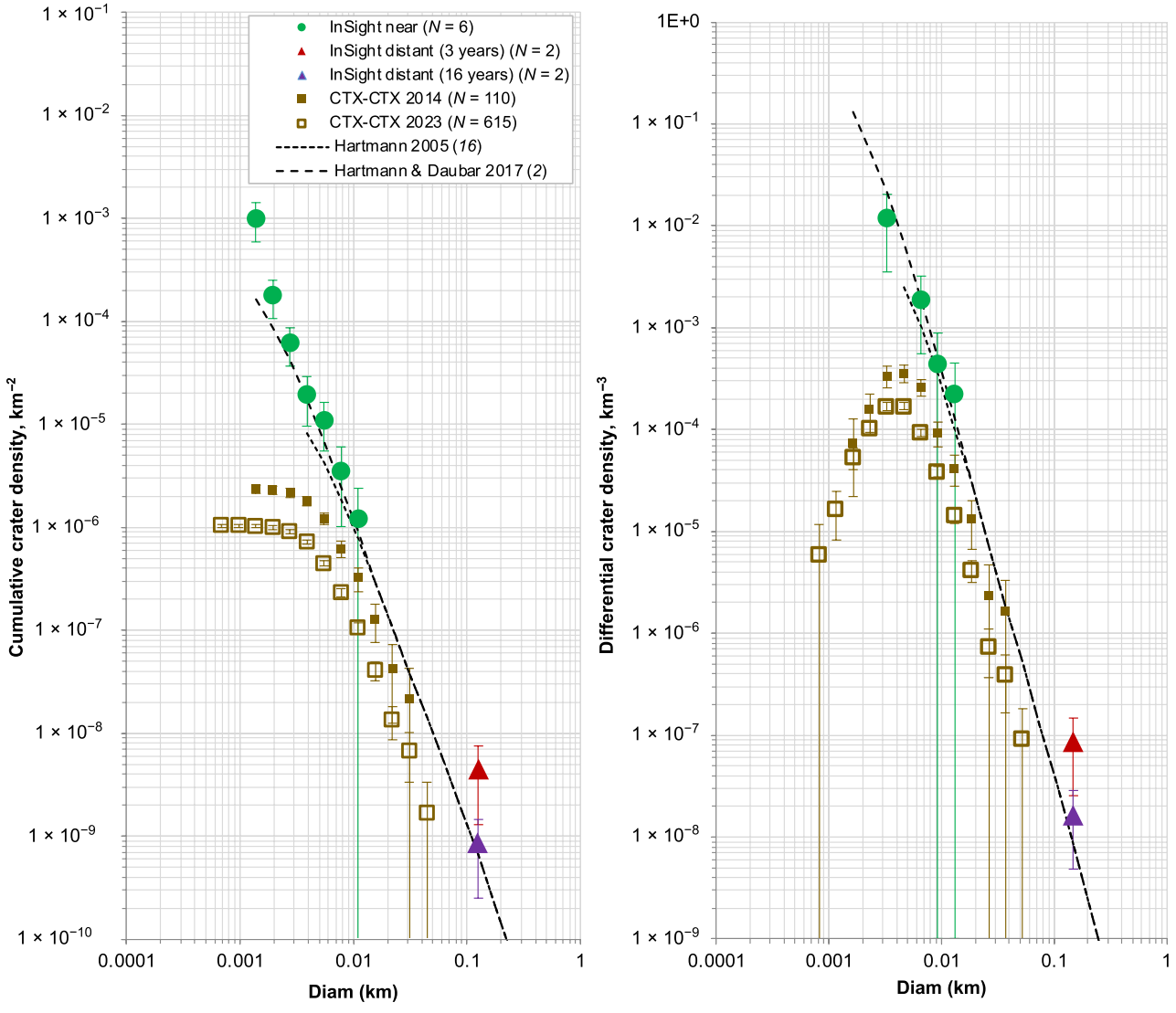

Fig. 2. Impact rates on Mars derived from different data sources. Annualized cumulative (*37*) (**left**) and differential (*38*) (**right**) SFDs showing the current impact rate. Impacts detected using an updated global dataset of CTX before and after constraining images (*7*) (brown open squares) are compared to previous results (*15*) (brown filled squares) as well as those detected using seismic-acoustic chirp signals (green filled circles) and those detected teleseismically (red and purple triangles normalized assuming temporal baselines of 3.1 and 16 years, respectively). Observed annual impact densities are compared to 1-year isochrons predicted based on lunar chronology adapted to Mars (*2*, *16*). Effective diameters are used for clusters; craters are combined in $\sqrt{2}$ diameter bins. Datasets are each scaled to the relevant ATF (see Materials and Methods). Error bars are standard counting errors.

topography (*11*)]. A recent work applied machine learning techniques to find new impacts and found 69 new impact sites that had previously been undetected, and that work examined just a small fraction of the identified candidates (*19*). These detections indicate a largely untapped potential application for more in-depth search of CTX images for new impacts.

When we compare the orbitally measured impact rate to that detected by InSight using nearby events, we conclude that the rate InSight measures is several times higher. This is especially evident at the smallest sizes. At D < ~10 m, we see a marked rollover in the cumulative size-frequency distribution (SFD) and drop-off in the differential SFD of orbitally detected impacts with decreasing crater diameter. This is at least partly due to resolution limitations causing fewer small impacts to be detected in images. In the seismic detections, we do not see such a resolution rollover or drop-off. Atmospheric filtering, deceleration, and ablation will reduce the small crater impact rate at diameters D < ~30 m (*17*, *18*), but such a marked rollover/drop-off is expected only for crater diameters of <1 m (*18*). The difference between orbital and seismic observations at larger sizes (D > ~10 m) could indicate a change in impact rate over a timescale of years to decades but more likely stems from the completeness of the respective datasets. It is also possible that the calculated ATF for the nearby seismic detection is an underestimation, which would result in a higher inferred impact rate than the one we derive. The presence of a seismic-acoustic chirp in the seismic data robustly eliminates false positives in the list of seismically

detected nearby impacts. We are therefore confident that the impacts detected in this manner represent the lower bound of impact frequency nearby.

The coincidence of the InSight-detected impacts with the Hartmann model prediction is remarkable. Those model isochrons are known to include an unquantified contribution of unrecognized, distant secondaries (*2*, *16*, *20*). While that contribution may average out over a long time interval during which many secondary-forming events happen, that is not the case for the crater size range and timescale relevant for the rates presented here. Seismically detected impacts are uncontaminated by secondaries, so they represent a minimum measurement of the primary impact flux. It is implausible that older surfaces are free of secondary craters; hence, models of the long-term total primary plus secondary crater population need to be adjusted upward. Applying such an adjusted model to crater counts of older surfaces would result in younger model ages for those surfaces.

In addition, on older terrains, it is not possible to reconstitute clusters of primary impacts into their combined effective diameters, as is possible with recent crater observations. This is because the surficial albedo markings formed in the impact event fade relatively quickly (*21*). Instead, the individual craters in an older cluster of primaries would be counted as separate impact events rather than one. This would steepen the resulting long-term crater SFD (*6*). This effect on the SFD may be somewhat compensated for by correcting for the unintentional inclusion of unrecognized secondaries, as discussed above.

The two distant impacts that InSight detected are the largest natural craters known to have formed anywhere in the Solar System in the era of space exploration. [Note that a crater with a diameter of 148 m (*5*) previously reported as new was later revealed to contain well-developed aeolian ripples, indicating a much older formation time (*22*).] Calculating a long-term rate based on two impacts is obviously problematic. However, we also cannot discount them completely. We present an impact rate based on these craters here, but it should be viewed with caution. Particularly, in this case, the relevant timescale over which the rate is calculated (the time used in the ATF scaling) is highly influential. The seismic events generated by these impacts are amongst the largest in the catalog and could have been observed at any time while the seismometer was recording (*23*), which includes 3.1 Earth years of data. InSight could be considered necessary to the discovery of these large impacts because they were found after focused regional and temporal searches in orbital images that were prompted by seismic findings. The cratering rate implied by the timescale of InSight's seismic search is substantially higher than the Hartmann cratering rate. Craters with larger diameters are considered to be better constrained in the martian cratering rate model as the relevant counts use older terrains and are less fraught with the complications of cluster formation (*6*). It is therefore unlikely that this high rate is representative of the long-term average. On the other hand, if the full timeframe of the MRO mission thus far (16.1 Earth years) is used for the ATF scaling, then the resulting rate is very close to that predicted by the martian cratering rate model. If the longer timeframe is used for scaling, then no additional explanation is needed as this is quite close to the model prediction.

As an extreme, we consider the time between the two large impact events, which is just 97 Earth days. If the two events were entirely uncorrelated and randomly distributed in time, then we could use a Poisson distribution to model the impact frequency. [This is a simplification, most notably because the impact rate is likely elevated near aphelion due to the proximity to the main asteroid belt (*1*, *24*, *25*).] Given a recurrence interval of 10.645 Earth years for this size range (diameters of 125 to 176 m) based on the Hartmann production function (*16*), there is only a 0.03% chance of two impacts of this size happening within 97 days (fig. S1). Within the InSight mission timeframe (3.1 Earth years), the probability of getting exactly two impacts is 3%. However, over the full timeframe of the MRO mission thus far (16.1 Earth years), there is a 25% chance that two impacts would have occurred. If the Hartmann production function was an underestimate of the current impact rate, as indicated by the InSight data as discussed above, then these probabilities would all increase somewhat.

The unlikely coincidence in timing of the two large impacts could be explained if the two events were related in some way. For example, it is possible that the two impacts were caused by fragments of a larger asteroid that recently broke up due to tidal stresses during a close approach with Mars or impact fragmentation on their progenitor. However, the time separation is large enough that there is not an obvious orbital association (i.e., Mars traveled about an eighth of the way around its orbit between the two events).

We find two indications of a higher recent impact rate as measured by InSight: The nearby impacts have an SFD higher than the primary-only chronology model (Fig. 3) and the two large distant impacts possibly show a higher rate than models predict. If these indications of a higher recent impact rate are correct, then we could imagine several sources of an enhanced impactor population. This could be evidence of a recent asteroid breakup and subsequent gravitational capture of two or more decameter-sized bodies. A relationship to a cometary stream can be dismissed for several reasons: No known meteoroid showers coincide with this timing within 10° L_S (*26*); 97 days is much longer than the expected length of a meteor shower on Mars [10 to 50 hours (*27*)]; and particle sizes in a cometary debris stream are generally much smaller than the impactors that created these new craters (*28*). A recent impact into Phobos or Deimos could have ejected a material that then impacted Mars over a short time period; however, such an impact would have had to be substantially larger than even these two large craters, which is exceedingly unlikely for those small targets.

It is entirely possible that other impact-generated signals remain unrecognized in the marsquake catalog. Zenhäusern *et al.* (*29*) examined the hypothesis that all InSight events in the very high frequency (VF) category are caused by impacts. These are a category of marsquake with common characteristics and a shallow but as yet uncertain source mechanism. The six smallest confirmed impacts of the eight discussed here are all associated with a VF-type marsquake. The resulting impact rate implied by the rate of all VF events is very similar to the rate reported here: several times higher than that of previous imaging-only studies and similar to cratering models that include unrecognized field secondaries (Fig. 3). The close agreement between the impact rate implied by VF events and the rate measured by confirmed impacts further supports the idea that the VF group of seismic events can be largely attributed to impacts. The best-fit power law slope of the cumulative VF event impact rate (−2.35) is lower than that of the orbitally confirmed seismic impact rate near InSight (−3.06), indicating that some very small impact events might as yet be unrecognized in the InSight catalog.

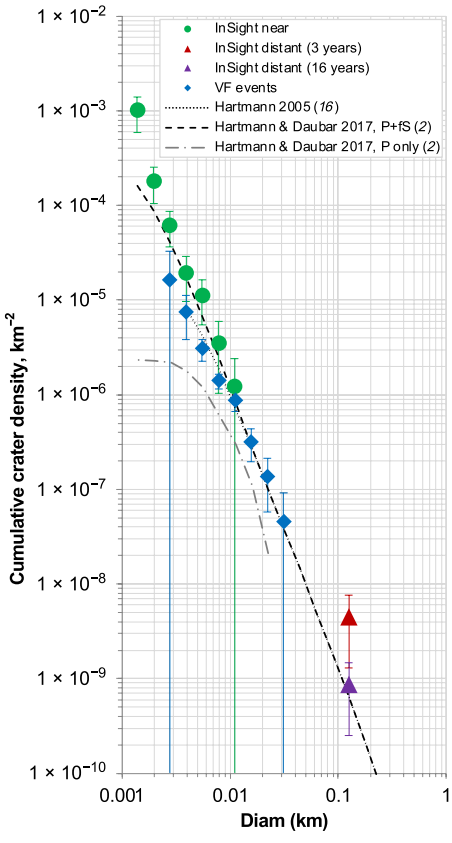

Fig. 3. Impact rates on Mars measured by InSight. Cumulative SFD showing the current annual impact rate using confirmed impacts nearby (green circles) and distant (red and purple triangles) to the lander, compared to the rate of VF events translated into equivalent impact sizes (blue diamonds) (*29*). One-year model isochrons are shown for comparison (*2*, *16*). All other details as in Fig. 2.

VF events are predicted to correspond to crater sizes 3 to 40 m in diameter, located up to 45° (~2700 km) away from the lander. To date, only small/local or large/global impacts have been detected both orbitally and seismically. This is because the small/local impacts were recognized due to their distinctive seismic-acoustic "chirp" signals, which have distance-limited detection (see Materials and Methods), and large/global impacts are rare enough that none happened to occur close to InSight. The VF event dataset would fill a portion of the gap in both distance and crater size between the confirmed impacts (Fig. 3). However, there is still a "deficit" of new craters with diameters of ~50 to 125 m. Recurrence intervals for this size range are only on the order of several Earth years [0.47 years for $D > 44.2$ m, 1.34 years for $D > 62.5$ m, and 3.71 years for $D > 88.3$ m using the Hartmann cratering model (*16*); these recurrence times would be shorter if the primary rate was higher]. There are almost certainly more new craters in this size range that have formed in the past few years, which have not yet been identified in the data. The latest image-based catalog (*7*) only has seven new impacts with $D_{eff} > 48$ m, but if the model rate was consistent for these sizes, then this suggests that there should have been ~30 impacts of this size across Mars during MRO's time of observing and 6 to 7 during InSight's time of observing. To be missed in MRO's orbital data, these could be located in areas where extended blast zones do not form, such as low-albedo/low-thermal inertia regions (*7*), and/or they have just been unrecognized thus far. Impacts of this size would likely have been detected globally with SEIS (*8*). Thus, to be missed in InSight's seismic data, these could have occurred during times when the seismometer data were extremely noisy, or they could have frequency and/or source characteristics that have not yet been recognized to be consistent with an impact source.

Seismic studies of Mars by InSight have revealed an additional dimension to the red planet. Our view of martian cratering, in particular, has evolved with these new data that reveal the small impact rate more completely than remote sensing from orbit has allowed in the past. Seismic data have proven to be a powerful tool in this regard as it has been demonstrated that (i) large teleseismic impact events can be detected globally, despite noise levels, and (ii) a seismometer can identify and locate impacts within a few hundred kilometers through the presence of a seismic-acoustic chirp signal. The latter is relevant to any planet with an atmosphere and thus may be applicable to future geophysical investigations of Titan or Venus for example. In the future, an array of seismometers would be an effective way to monitor the current impact rate on other planetary bodies. This is an additional aspect of the scientific value of geophysical data to our understanding of other planets.

MATERIALS AND METHODS

Crater measurements

Following a previously published method (*6*), the full catalog of new impacts was narrowed down to include those with CTX images as both before and after constraints, within dusty areas of Mars. Diameters and before/after image constraints of CTX-CTX constrained craters were taken from the Daubar *et al.* catalog (*7*) with updates as listed in data S1. Diameters of seismically detected impact craters (Table 1) were measured on RED HiRISE reduced data record (RDR) products (25 cm/pixel) (*22*) in (*30*) ArcGIS using the three-point tool of the CraterTools plugin (*31*). Uncertainty on the individual crater diameter measurements is less than a few pixels or 0.5 m. Individual diameters of craters in simultaneously forming clusters were combined using an effective diameter, the size of the crater that would have formed if no atmospheric fragmentation had occurred. This is defined as $D_{eff} = (\sum D_i^3)^{1/3}$, where the sum is over all individual crater diameters of >1 m in the cluster, D_i (*6*). This approximation is based on scaling for strength-dominated impacts and has been shown to be within 80% of the unfragmented diameter (the diameter of the crater that would have formed had it not broken up in the atmosphere) for $D_{eff} < 1$ m, and D_{eff} is within error bars of the unfragmented diameter for $D_{eff} > 10$ m (*18*).

Area-time factor

The ATF is used to normalize the SFD of crater diameters to produce a cratering rate per unit time per unit area, following a previously developed method (*6*). This method identifies areas over which new impacts could have been detected in CTX images. Each unit area is multiplied by the time difference between successive images and the total summed to derive a factor by which to scale the measured SFD. For the CTX-CTX constrained impacts, the Planetary Data System (PDS) catalog release mrox_4015 was used to calculate the ATF as that release contains images taken through 2021-01-26T15:51:09.236, and the latest "after" image among the CTX-CTX constrained impact sites in the latest catalog (*7*) was

Table 1. InSight seismic event names (*41*) and details for each seismically detected impact on Mars.

InSight event designator	Distance to InSight (km) (*11*)	Crater diameter (m) (effective diameter for clusters)	HiRISE observation ID
S0533a	286.3	11.9 (cluster) (*10*)	ESP_070864_1895
S0793a	91.0	3.9 (single) (*10*)	ESP_070073_1845
S0981c	240.5	7.2 (single) (*10*)	ESP_072644_1805
S0986c	85.0	6.1 (cluster) (*10*)	ESP_072222_1840
S1000a	7475.9	140 (cluster) (*13*)	ESP_073522_2185
S1034a	48.2	9.2 (single) (*11*)	ESP_074701_1840
S1094b	3462.0	150 (single) (*13*)	ESP_073077_2155
S1160a	59.6	3.2 (cluster) (*11*)	ESP_076877_1850

dated 2021-01-26T00:56:23.636. We limit the search area to where the dust cover index (DCI) (*32*) is <0.96, as was done previously (*6*), because the detected impacts are found mainly in dusty regions. Latitudes were also limited to ±60° due to seasonal processes erasing new impact blast zones quickly in the polar regions (*21*, *33*), leading to incompleteness of new impact detections in those regions. These limits were used on the imaging data used to calculate the ATF as well as to select the impact sites included in the SFD.

For the InSight-detected impacts, ATF values are calculated by considering the time over which it would have been possible to detect them and the estimated area over which each type of event was detectable. The teleseismic events are large enough that they would have been seismically detectable anywhere on Mars; thus, for these impacts, we use the entire surface of Mars as the relevant area. Those two distant impacts are also so large that it is possible they could have been detected using orbital images at any point in the MRO mission while the Mars Color Imager (MARCI) has been imaging. Although it is uncertain how thoroughly MARCI is searched for new impacts, we used the full length of that mission to date (16.1 Earth years) as an upper limit on the possible detection time period as well as the time that the InSight seismometer SEIS (*8*) could have detected them. For these large impacts, the applicable time is the full period of data recorded by SEIS. This includes data from the time the wind and thermal shield was placed on top of SEIS on 2 February 2019 until the final data were returned on 13 December 2022, after which communications were lost. Over the mission, a total of 3.1 Earth years of data were recorded as the time SEIS could be powered on was reduced in the final year of operations due to power constraints.

For local impacts, the presence of the seismic-acoustic chirp appears to be confirmatory of an impact event. The scaling time for the local impact detections is, therefore, the duration of data where the noise level was low enough to observe the chirp. To calculate this, we calculated the root mean square (RMS) seismic velocity of the vertical component in the 0.4- to 2-Hz range (where the impact acoustic chirp is most prominent). The threshold for which the chirp signal can be observed is defined as $A_{vz} \leq 2.0 \times 10^{-10}$ m/s. Figure 4 shows the cumulative distribution function (CDF) of the RMS seismic velocity over the mission, indicating that the noise level was below the threshold for 22% of the mission. This leads to a total time of 0.7 Earth years for which the detected local events could be confirmed as impacts by observation of the seismic-acoustic chirp.

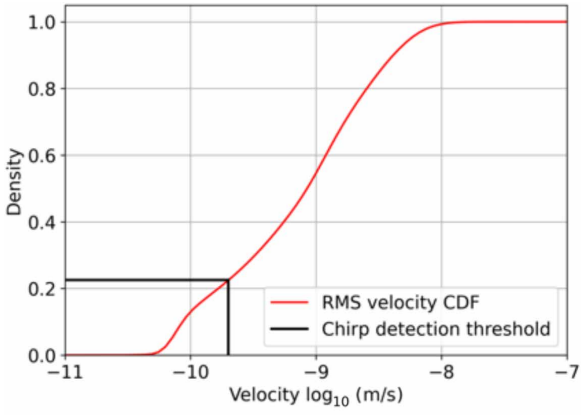

Fig. 4. Cumulative time InSight ambient seismic noise was below a given level. CDF of the vertical component of the RMS seismic velocity in the 0.4- to 2.0-Hz bandwidth over the whole InSight mission. Between marsquakes, this velocity is the ambient seismic noise level. Black box indicates the region below the detection threshold for the seismic-acoustic chirp of $A_{vz} \leq 2.0 \times 10^{-10}$ m/s. This represents 22% of the total mission data.

The impact acoustic chirps are detectable out to at least the distance to the farthest one (289 km). This is a lower limit of detectability though, so to improve on this, we calculate the theoretical detectability limit of chirps from various size impacts at different distances and use that to scale each diameter bin individually. The distance at which acoustic-seismic chirp signals from a given impact are detectable depends on the momentum of the impact. To calculate this distance for each of the diameter bins in the SFD, we established a scaling law between crater diameter and acoustic signal recorded by SEIS through vertical ground velocity (in meters per second) in the 0.5- to 1.5-Hz frequency range. The acoustic energy E is related to the crater diameter D_c according to the formula $E = \gamma D_c^{3.3}$, with γ a proportionality parameter to be estimated. The exponent 3.3 is deduced assuming that the acoustic energy has a similar dependence on crater diameter as the seismic moment. This dependence was estimated by scaling numerical simulations with previous impact records (*34*). The exponent in this power law is also broadly consistent with empirical relationships derived from nuclear explosion data that predict an exponent of 3 (*35*).

The propagation effects on the amplitude of acoustic waves trapped in the atmosphere waveguide close to the surface is taken into account through the following formula

$$A_{vz}(D_c, d) = E\frac{\beta}{\sqrt{d}}e^{-\alpha d} = \gamma D_c^{3.3}\frac{\beta}{\sqrt{d}}e^{-\alpha d} \quad (1)$$

The scaling law with distance (d) is obtained from trapped waves propagating close to the surface, and the dimensionless attenuation parameter α at 1 Hz on Mars close to the surface is estimated to be 10^{-5}, at pressure and temperature conditions of Mars surface during nighttime (*36*). Then, we estimate for the unknown product $B = \gamma\beta$ through the following formula, using the six nearby impact events recorded by SEIS

$$B = \gamma\beta = A_{vz}\sqrt{d}D_c^{-3.3}e^{\alpha d} \quad (2)$$

The results are in good agreement with each other, averaging to a value of B of $2.65 \times 10^{-8} \pm 7.15 \times 10^{-9}$. The stability of the B estimates as a function of distance can also be used to constrain the attenuation parameter α in the range 0.5×10^{-6} to 2×10^{-5}. We use the average value for B to then calculate the signal strength for various size impact craters at different distances using Eq. 2 (Fig. 5). The intersection of these curves for a given crater diameter with the noise threshold of $A_{vz} = 2.0 \times 10^{-10}$ m/s is used as the maximum distance at which an acoustic signal from that size impact would be above the noise level. This distance was then used as the radius (r) along the surface of a sphere with Mars' mean planetary radius (R) to calculate the area (A) in the ATF, using the formula $A = 2\pi R^2\left(1 - \cos\frac{r}{R}\right)$. Note that this value is different for each diameter bin. Resulting ATF values for all datasets are shown in Table 2.

SFD plotting methods

SFD plots are constructed according to standard techniques (*37*–*39*), with the added feature of normalization by time via the ATF as has been done previously (*5*, *6*, *40*). In this application, however, the ATF value varies by diameter D for the seismically detected impacts because the detectability varies by diameter and distance, as discussed above and enumerated in Table 2. This complicates the differential SFD, which is normally defined in relation to the cumulative SFD $C(D)$ as (*37*)

$$F(D) = \frac{[C(D_a) - C(D_b)]}{(D_b - D_a)} \quad (3)$$

for the bin with diameter limits D_a and D_b ($D_b > D_a$), and $D = \sqrt{D_a D_b}$. Here, we are plotting $C(D)$/ATF instead of merely $C(D)$ to get an annualized global impact rate. If the ATF is also a function of D, then the differential becomes

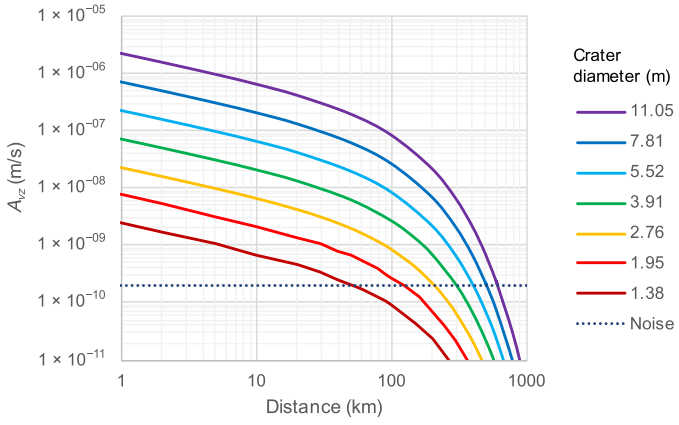

Fig. 5. Amplitude of the acoustic signal for a given size impact as a function of distance. Amplitude of the vertical component of velocity (A_{vz}, in meters per second) of the acoustic wave as a function of distance (in kilometers) from the impact point, for various sized impact craters (colored solid lines, labeled with diameter in meters). These diameters were chosen to match the lower bin boundaries for the SFDs plotted in Figs. 2 and 3.

Table 2. ATF values for various datasets used in SFDs. N/A, not applicable.

Dataset, scenario	Area (km²)	Time (Earth years)	Resulting ATF (km² yr)
Large distant two impacts	1.44×10^{08} (total area of Mars)	16 (MRO dataset length)	2.31×10^{09}
		3.1 (time SEIS recording data)	1.86×10^{08}
Small nearby impacts, diameter bin minimum			
D_c 1.38 m	8.58×10^{03}	0.7 (time SEIS noise below chirp threshold)	6.00×10^{03}
D_c 1.95 m	4.79×10^{04}		3.35×10^{04}
D_c 2.76 m	1.40×10^{05}		9.79×10^{04}
D_c 3.91 m	2.96×10^{05}		2.07×10^{05}
D_c 5.52 m	5.20×10^{05}		3.64×10^{05}
D_c 7.81 m	8.16×10^{05}		5.71×10^{05}
D_c 11.05 m	1.18×10^{06}		8.29×10^{05}
D_c 15.63 m	1.63×10^{06}		1.14×10^{06}
CTX-CTX constrained impacts, lat < 60, DCI < 0.96			
2014	N/A	N/A	4.68×10^{07}
2023	N/A	N/A	3.94×10^{08}

$$F'(D) = \frac{[C(D_a)/\mathrm{ATF}(D_a) - C(D_b)/\mathrm{ATF}(D_b)]}{(D_b - D_a)} \quad (4)$$

Normally, in cases where adjacent bins in the cumulative SFD are equal [i.e., $C(D_a) = C(D_b)$], the differential value is zero. However, if the above definition (Eq. 4) is used in a case such as this where ATF varies with D, then adjacent bins could have equal values of $C(D)$ but differing ATF values, resulting in a nonzero value for $F(D)$. It would be misleading to show a nonzero data point in a diameter bin where the number of craters is actually zero. Thus, we instead plot the differential SFD using

$$F'(D) = \frac{[C(D_a) - C(D_b)]/\mathrm{ATF}(D_{gm})}{(D_b - D_a)} \quad (5)$$

In the case where ATF does not vary with D, Eq. 5 is equivalent to Eq. 4 but, in our application of varying ATF, still results in the expected zero values for $F'(D)$ where $C(D_a) = C(D_b)$. We use the ATF value at the geometric mean of the bin extrema (D_{gm}) in Eq. 5 for $F'(D)$. This is because SFD points are plotted against the geometric mean of the bin extrema in the differential plot, which reduces bias that would be introduced were the points to be plotted against the bin extrema or center (*38*). SFD points are plotted against the bin minima in the cumulative plot, which avoids that bias.

Supplementary Materials

This PDF file includes:
Fig. S1
Legend for data S1

Other Supplementary Material for this manuscript includes the following:
Data S1

REFERENCES AND NOTES

1. B. A. Ivanov, Mars/moon cratering rate ratio estimates. *Space Sci. Rev.* **96**, 87–104 (2001).
2. W. K. Hartmann, I. J. Daubar, Martian cratering 11. Utilizing decameter scale crater populations to study Martian history. *Meteorit. Planet. Sci.* **52**, 493–510 (2017).
3. D. Robertson, P. Pokorný, M. Granvik, L. Wheeler, C. Rumpf, Latitude variation of flux and impact angle of asteroid collisions with Earth and the Moon. *Planet. Sci. J.* **2**, 88 (2021).
4. A. Lagain, M. Kreslavsky, D. Baratoux, Y. Liu, H. Devillepoix, P. Bland, G. K. Benedix, L. S. Doucet, K. Servis, Has the impact flux of small and large asteroids varied through time on Mars, the Earth and the Moon? *Earth Planet. Sci. Lett.* **579**, 117362 (2022).
5. M. C. Malin, K. S. Edgett, L. V. Posiolova, S. M. McColley, E. Z. Noe Dobrea, E. Z. N. Dobrea, Present-day impact cratering rate and contemporary gully activity on Mars. *Science* **314**, 1573–1577 (2006).
6. I. J. Daubar, A. S. McEwen, S. Byrne, M. R. Kennedy, B. A. Ivanov, The current martian cratering rate. *Icarus* **225**, 506–516 (2013).
7. I. J. Daubar, C. M. Dundas, A. S. McEwen, A. Gao, D. Wexler, S. Piqueux, G. S. Collins, K. Miljkovic, T. Neidhart, J. Eschenfelder, G. D. Bart, K. L. Wagstaff, G. Doran, L. Posiolova, M. Malin, G. Speth, D. Susko, A. Werynski, New craters on Mars: An updated catalog. *J. Geophys. Res Planets* **127**, e07145 (2022).
8. P. Lognonné, W. B. Banerdt, D. Giardini, W. T. Pike, U. Christensen, P. Laudet, S. de Raucourt, P. Zweifel, S. Calcutt, M. Bierwirth, K. J. Hurst, F. Ijpelaan, J. W. Umland, R. Llorca-Cejudo, S. A. Larson, R. F. Garcia, S. Kedar, B. Knapmeyer-Endrun, D. Mimoun, A. Mocquet, M. P. Panning, R. C. Weber, A. Sylvestre-Baron, G. Pont, N. Verdier, L. Kerjean, L. J. Facto, V. Gharakanian, J. E. Feldman, T. L. Hoffman, D. B. Klein, K. Klein, N. P. Onufer, J. Paredes-Garcia, M. P. Petkov, J. R. Willis, S. E. Smrekar, M. Drilleau, T. Gabsi, T. Nebut, O. Robert, S. Tillier, C. Moreau, M. Parise, G. Aveni, S. B. Charef, Y. Bennour, T. Camus, P. A. Dandonneau, C. Desfoux, B. Lecomte, O. Pot, P. Revuz, D. Mance, J. tenPierick, N. E. Bowles, C. Charalambous, A. K. Delahunty, J. Hurley, R. Irshad, H. Liu, A. G. Mukherjee, I. M. Standley, A. E. Stott, J. Temple, T. Warren, M. Eberhardt, A. Kramer, W. Kühne, E.-P. Miettinen, M. Monecke, C. Aicardi, M. André, J. Baroukh, A. Borrien, A. Bouisset, P. Boutte, K. Brethomé, C. Brysbaert, T. Carlier, M. Deleuze, J. M. Desmarres, D. Dilhan, C. Doucet, D. Faye, N. Faye-Refalo, R. Gonzalez, C. Imbert, C. Larigauderie, E. Locatelli, L. Luno, J.-R. Meyer, F. Mialhe, J. M. Mouret, M. Nonon, Y. Pahn, A. Paillet, P. Pasquier, G. Perez, R. Perez, L. Perrin, B. Pouilloux, A. Rosak, I. S. de Larclause, J. Sicre, M. Sodki, N. Toulemont, B. Vella, C. Yana, F. Alibay, O. M. Avalos, M. A. Balzer, P. Bhandari, E. Blanco, B. D. Bone, J. C. Bousman, P. Bruneau, F. J. Calef, R. J. Calvet, S. A. D'Agostino, G. de los Santos, R. G. Deen, R. W. Denise, J. Ervin, N. W. Ferraro, H. E. Gengl, F. Grinblat, D. Hernandez, M. Hetzel, M. E. Johnson, L. Khachikyan, J. Y. Lin, S. M. Madzunkov, S. L. Marshall, I. G. Mikellides, E. A. Miller, W. Raff, J. E. Singer, C. M. Sunday, J. F. Villalvazo, M. C. Wallace, D. Banfield, J. A. Rodriguez-Manfredi, C. T. Russell, A. Trebi-Ollennu, J. N. Maki, E. Beucler, M. Böse, C. Bonjour, J. L. Berenguer, S. Ceylan, J. Clinton, V. Conejero, I. J. Daubar, V. Dehant, P. Delage, F. Euchner, I. Estève, L. Fayon, L. Ferraioli, C. L. Johnson, J. Gagnepain-Beyneix, M. P. Golombek, A. Khan, T. Kawamura, B. Kenda, P. Labrot, N. Murdoch, C. Pardo, C. Perrin, L. Pou, A. Sauron, D. Savoie, S. Stähler, E. Stutzmann, N. A. Teanby, J. Tromp, M. van Driel, M. A. Wieczorek, R. Widmer-Schnidrig, J. Wookey, SEIS: Insight's seismic experiment for internal structure of Mars. *Space Sci. Rev.* **215**, 12 (2019).
9. W. B. Banerdt, S. Smrekar, D. Banfield, D. Giardini, M. P. Golombek, C. Johnson, P. Lognonné, A. Spiga, T. Spohn, C. Perrin, S. Stähler, D. Antonangeli, S. Asmar, C. Beghein, N. Bowles, E. Bozdag, P. Chi, U. Christensen, C. John, G. S. Collins, I. J. Daubar, V. Dehant, M. Drilleau, M. Fillingim, W. Folkner, R. F. Garcia, J. B. Garvin, J. Grant, M. Grott, J. Grygorczuk, T. Hudson, J. Irving, G. Kargl, T. Kawamura, S. Kedar, S. King, B. Knapmeyer-Endrun, M. Knapmeyer, M. T. Lemmon, R. D. Lorenz, J. Maki, L. Margerin, S. McLennan, C. Michaut, D. Mimoun, A. Mittelholz, A. Mocquet, P. Morgan, N. Mueller, N. Murdoch, S. Nagihara, C. E. Newman, F. Nimmo, M. Panning, W. T. Pike, A.-C. Plesa, S. Rodriguez, J.-A. Rodriguez-Manfredi, C. Russell, N. C. Schmerr, M. Siegler, S. Stanley, E. Stutzmann, N. A. Teanby, J. Tromp, M. van Driel, N. H. Warner, R. Weber, M. A. Wieczorek, Initial results from the insight mission on Mars. *Nat. Geosci.* **13**, 183–189 (2020).
10. R. F. Garcia, I. J. Daubar, É. Beucler, L. V. Posiolova, G. S. Collins, P. Lognonné, L. Rolland, Z. Xu, N. Wójcicka, A. Spiga, B. Fernando, G. Speth, L. Martire, A. Rajšić, K. Miljković, E. K. Sansom, C. Charalambous, S. Ceylan, S. Menina, L. Margerin, R. Lapeyre, T. Neidhart, N. A. Teanby, N. C. Schmerr, M. Bonnin, M. Froment, J. F. Clinton, O. Karatekin, S. C. Stähler, N. L. Dahmen, C. Durán, A. Horleston, T. Kawamura, M. Plasman, G. Zenhäusern, D. Giardini, M. Panning, M. Malin, W. B. Banerdt, Newly formed craters on Mars located using seismic and acoustic wave data from InSight. *Nat. Geosci.* **15**, 774–780 (2022).
11. I. J. Daubar, B. Fernando, R. Garcia, G. Peter, G. Zenhaeusern, N. Wójcicka, N. Teanby, S. Staehler, L. Posiolova, A. Horleston, G. Collins, C. Charalambous, J. Clinton, M. Banks, P. Lognonne, M. Panning, W. B. Banerdt, Two seismic events from InSight confirmed as new impacts on Mars. *Planet. Sci. J.* **4**, 175 (2023).
12. J. Clinton, D. Giardini, M. Böse, S. Ceylan, M. van Driel, F. Euchner, R. F. Garcia, S. Kedar, A. Khan, S. C. Stähler, W. B. Banerdt, P. Lognonné, E. Beucler, I. J. Daubar, M. Drilleau, M. P. Golombek, T. Kawamura, M. Knapmeyer, B. Knapmeyer-Endrun, D. Mimoun, A. Mocquet, M. Panning, C. Perrin, N. A. Teanby, The Marsquake service: Securing daily analysis of SEIS data and building the Martian seismicity catalogue for InSight. *Space Sci. Rev.* **214**, 133 (2018).
13. L. V. Posiolova, P. Lognonné, W. B. Banerdt, J. Clinton, G. S. Collins, T. Kawamura, S. Ceylan, I. J. Daubar, B. Fernando, M. Froment, D. Giardini, M. C. Malin, K. Miljković, S. C. Stähler, Z. Xu, M. E. Banks, É. Beucler, B. A. Cantor, C. Charalambous, N. Dahmen, P. Davis, M. Drilleau, C. M. Dundas, C. Durán, F. Euchner, R. F. Garcia, M. Golombek, A. Horleston, C. Keegan, A. Khan, D. Kim, C. Larmat, R. Lorenz, L. Margerin, S. Menina, M. Panning, C. Pardo, C. Perrin, W. T. Pike, M. Plasman, A. Rajšić, L. Rolland, E. Rougier, G. Speth, A. Spiga, A. Stott, D. Susko, N. A. Teanby, A. Valeh, A. Werynski, N. Wójcicka, G. Zenhäusern, Largest recent impact craters on Mars: Orbital imaging and surface seismic co-investigation. *Science* **378**, 412–417 (2022).
14. I. J. Daubar, P. Lognonné, N. A. Teanby, K. Miljković, J. Stevanović, J. Vaubaillon, B. Kenda, T. Kawamura, J. F. Clinton, A. S. Lucas, M. Drilleau, C. Yana, G. S. Collins, D. Banfield, M. P. Golombek, S. Kedar, N. C. Schmerr, R. F. Garcia, S. Rodriguez, T. V. Gudkova, S. May, M. Banks, J. N. Maki, E. Sansom, F. Karakostas, M. Panning, N. Fuji, J. Wookey, M. van Driel, M. T. Lemmon, V. Ansan, M. Böse, S. Stähler, H. Kanamori, J. E. Richardson, S. E. Smrekar, W. B. Banerdt, Impact-seismic investigations of the InSight mission. *Space Sci. Rev.* **214**, doi.org/10.1007/s11214-018-0562-x (2018).
15. I. J. Daubar, A. S. McEwen, S. Byrne, M. A. Kreslavsky, L. Saper, M. R. Kennedy, New dated impacts on Mars and an updated current cratering rate, in *Eighth International Conference on Mars* (USRA, 2014), p. 1007.
16. W. K. Hartmann, Martian cratering 8: Isochron refinement and the chronology of Mars. *Icarus* **174**, 294–320 (2005).
17. G. S. Collins, E. L. Newland, D. Schwarz, M. Coleman, S. Mcmullan, I. J. Daubar, K. Miljković, T. Neidhart, E. K. Sansom, Meteoroid fragmentation in the martian atmosphere and the formation of crater clusters. *J. Geophys. Res. Planets* **127**, e2021JE007149 (2022).
18. J.-P. Williams, A. V. Pathare, O. Aharonson, The production of small primary craters on Mars and the Moon. *Icarus* **235**, 23–36 (2014).
19. K. L. Wagstaff, I. J. Daubar, G. Doran, M. J. Munje, V. T. Bickel, A. Gao, J. Pate, D. Wexler, Using machine learning to reduce observational biases when detecting new impacts on Mars. *Icarus* **386**, 115146 (2022).

20. A. Lagain, G. K. Benedix, K. Servis, D. Baratoux, L. S. Doucet, A. Rajšic, H. A. R. Devillepoix, P. A. Bland, M. C. Towner, E. K. Sansom, K. Miljković, The Tharsis mantle source of depleted shergottites revealed by 90 million impact craters. *Nat. Commun.* **12**, 6352 (2021).
21. I. J. Daubar, C. M. Dundas, S. Byrne, P. E. Geissler, G. D. Bart, A. S. McEwen, P. S. Russell, M. Chojnacki, M. P. Golombek, Changes in blast zone albedo patterns around new martian impact craters. *Icarus* **267**, 86–105 (2016).
22. N. T. Bridges, P. E. Geissler, A. S. McEwen, B. J. Thomson, F. C. Chuang, K. E. Herkenhoff, L. P. Keszthelyi, S. Martínez-Alonso, Windy Mars: A dynamic planet as seen by the HiRISE camera. *Geophys. Res. Lett.* **34**, L23205 (2007).
23. A. E. Stott, R. F. Garcia, A. Chédozeau, A. Spiga, N. Murdoch, B. Pinot, D. Mimoun, C. Charalambous, A. Horleston, S. D. King, T. Kawamura, N. Dahmen, S. Barkaoui, P. Lognonné, W. B. Banerdt, Machine learning and marsquakes: A tool to predict atmospheric-seismic noise for the NASA InSight mission. *Geophys. J. Int.* **233**, 978–998 (2023).
24. I. J. Daubar, A. S. McEwen, S. Byrne, M. R. Kennedy, Seasonal variation in current martian impact rate, in *43rd Lunar and Planetary Science Conference (LPSC)* (LPSC, 2012), Abs. 2740.
25. Y. JeongAhn, R. Malhotra, On the non-uniform distribution of the angular elements of near-Earth objects. *Icarus* **229**, 236–246 (2014).
26. A. A. Christou, J. Oberst, V. Lupovka, V. Dmitriev, M. I. Gritsevich, The meteoroid environment and impacts on Phobos. *Planet. Space Sci.* **102**, 164–170 (2014).
27. A. A. Christou, J. Vaubaillon, "Numerical modeling of cometary meteoroid streams encountering Mars and Venus" in *Meteoroids: The Smallest Solar System Bodies* (NASA, 2011), pp. 26–30.
28. R. M. Suggs, D. E. Moser, W. J. Cooke, R. J. Suggs, The flux of kilogram-sized meteoroids from lunar impact monitoring. *Icarus* **238**, 23–36 (2014).
29. G. Zenhäusern, N. Wojcicka, S. Stähler, G. Collins, I. Daubar, M. Knapmeyer, S. Ceylan, J. Clinton, D. Giardini, Are high frequency marsquakes caused by meteoroid impacts? Implications for a seismically determined impact rate on Mars (2024); https://doi.org/10.21203/rs.3.rs-2742268/v1.
30. A. S. Mc Ewen, E. M. Eliason, J. W. Bergstrom, N. T. Bridges, C. J. Hansen, W. A. Delamere, J. A. Grant, V. C. Gulick, K. E. Herkenhoff, L. Keszthelyi, R. L. Kirk, M. T. Mellon, S. W. Squyres, N. Thomas, C. M. Weitz, Mars reconnaissance orbiter's high resolution imaging science experiment (HiRISE). *J. Geophys. Res. Planets* **112**, doi.org/10.1029/2005JE002605 (2007).
31. T. Kneissl, S. van Gasselt, G. Neukum, Map-projection-independent crater size-frequency determination in GIS environments—New software tool for ArcGIS. *Planet. Space Sci.* **59**, 1243–1254 (2011).
32. S. W. Ruff, P. R. Christensen, Bright and dark regions on Mars: Particle size and mineralogical characteristics based on Thermal Emission Spectrometer data. *J. Geophys. Res. Planets* **107**, 5127 (2002).
33. C. M. Dundas, M. T. Mellon, S. J. Conway, I. J. Daubar, K. E. Williams, L. Ojha, J. J. Wray, A. M. Bramson, S. Byrne, A. S. McEwen, L. V. Posiolova, G. Speth, D. Viola, M. E. Landis, G. A. Morgan, A. V. Pathare, Widespread exposures of extensive clean shallow ice in the midlatitudes of Mars. *J. Geophys. Res. Planets* **126**, e2020JE006617 (2021).
34. N. Wójcicka, G. S. Collins, I. D. Bastow, N. A. Teanby, K. Miljković, A. Rajšić, I. J. Daubar, P. Lognonné, The seismic moment and seismic efficiency of small impacts on Mars. *J. Geophys. Res. Planets* **125**, e2020JE006540 (2020).
35. S. Glasstone, P. J. Dolan, Eds., *The Effects of Nuclear Weapons* (U.S. Dept. of Defense and U.S. Dept. of Energy, 1977).
36. A. Petculescu, R. M. Lueptow, Atmospheric acoustics of Titan, Mars, Venus, and Earth. *Icarus* **186**, 413–419 (2007).
37. Crater Analysis Techniques Working Group, Standard techniques for presentation and analysis of crater size-frequency data. *Icarus* **37**, 467–474 (1979).
38. G. G. Michael, Planetary surface dating from crater size-frequency distribution measurements: Multiple resurfacing episodes and differential isochron fitting. *Icarus* **226**, 885–890 (2013).
39. C. I. Fassett, Analysis of impact crater populations and the geochronology of planetary surfaces in the inner solar system. *J. Geophys. Res. Planets* **121**, 1900–1926 (2016).
40. E. J. Speyerer, R. Z. Povilaitis, M. S. Robinson, P. C. Thomas, R. V. Wagner, V. Robert, Quantifying crater production and regolith overturn on the Moon with temporal imaging. *Nature* **538**, 215–218 (2016).
41. S. Ceylan, J. F. Clinton, D. Giardini, S. C. Stähler, A. Horleston, T. Kawamura, M. Böse, C. Charalambous, N. L. Dahmen, M. van Driel, C. Durán, F. Euchner, A. Khan, D. Kim, M. Plasman, J.-R. Scholz, G. Zenhäusern, E. Beucler, R. F. Garcia, S. Kedar, M. Knapmeyer, P. Lognonné, M. P. Panning, C. Perrin, W. T. Pike, A. E. Stott, W. B. Banerdt, The marsquake catalogue from InSight, sols 0–1011. *Phys. Earth Planet. In.* **333**, 106943 (2022).

Acknowledgments: We thank the InSight and MRO operations staff who planned, acquired, and processed the data used in this work. We thank L. Ostrach for useful comments on the text. A portion of the work was supported by the InSight Project at the Jet Propulsion Laboratory, California Institute of Technology, under a contract with the National Aeronautics and Space Administration (NASA). Any use of trade, firm, or product names is for descriptive purposes only and does not imply endorsement by the U.S. government. This is InSight contribution number 294. **Funding:** This work was supported by the NASA InSight PSP [grant 80NSSC20K0971 (I.J.D.)], NASA SSW [grant 80NSSC20K0789 (I.J.D.)], U.K. Space Agency [grants ST/S001514/1, ST/T002026/1, and ST/Y000102/1 (G.S.C. and N.WETH Zurich ETH+02 19-1: "Planet Mars" (G.Z. and S.C.S.), and CNES postdoctoral fellowship (A.E.S.). **Author contributions:** Conceptualization: I.J.D. and R.F.G. Methodology: I.J.D., R.F.G., and C.C. Investigation: I.J.D., A.E.S., B.F., and A.S.M. Visualization: I.J.D., A.E.S., and B.F. Supervision: A.S.M., P.L., and W.B.B. Discussion: I.J.D., G.S.C., N.W., G.Z., S.C.S., and D.G. Writing—original draft: I.J.D. Writing—review and editing: I.J.D., R.F.G., A.E.S., B.F., G.S.C., C.M.D., N.W., G.Z., A.S.M., S.C.S., and M.G. **Competing interests:** The authors declare that they have no competing interests. **Data and materials availability:** All data needed to evaluate the conclusions in the paper are present in the paper and/or the Supplementary Materials. SEIS waveform data and station metadata are available from the from the Institut de Physique du Globe de Paris Datacenter and Incorporated Research Institutions for Seismology Data Management Center at http://dx.doi.org/10.18715/SEIS.INSIGHT.XB_2016. Marsquake locations and metadata are available from the Mars Quake Service catalog (*40*) (https://doi.org/10.12686/a21) produced by the SEIS data service (*12*). HiRISE data are available from https://uahirise.org/, and CTX data are available on the NASA PDS (https://pds.nasa.gov).

Submitted 16 November 2023
Accepted 28 May 2024
Published 28 June 2024
10.1126/sciadv.adk7615